

# Optimization of High Altitude Long Endurance (HALE) Vehicle Subject to Flutter Speed Constraint

Kevin Roughen<sup>\*</sup>, Joe Robinson<sup>†</sup>, Myles Baker<sup>‡</sup>

*M4 Engineering, Inc., Long Beach, CA, 90807*

Zhang Liu<sup>§</sup>

*Woodland Hills, CA 91367*

**A class of air vehicles known as high altitude long endurance (HALE) has gained interest for a broad range of applications. Endurance requirements generally lead to vehicles with low mass and high aspect ratio wings. Such configurations are generally susceptible to aeroelastic effects including flutter. This work considers the aeroelastic behavior of a generic flying wing HALE vehicle configuration using generic stiffness and mass properties. An optimization study is presented that seeks to minimize penalties on trim drag and structural mass while satisfying a constraint on flutter speed. Optimization techniques employed include gradient based and a genetic algorithm. A Pareto Frontier is characterized that presents the set of designs that optimally satisfy the flutter constraint for a range of mass and drag penalties. This paper illustrates techniques that can be applied for optimization subject to aeroelastic constraints for general aircraft.**

## I. Introduction

Aeroelasticity involves the interaction of aerodynamics and structural dynamics. The nature of this interaction is that the aerodynamic pressures exert forces on the structure, while the structural deflections and velocities alter the aerodynamic pressure distribution. This interaction leads to a coupled aeroelastic system where neither the aerodynamic behavior nor the structural dynamic behavior can be addressed independently. Aeroelastic behavior is characterized as static or dynamic. Static aeroelastic phenomena include aeroelastic effects on static stability, load distribution, control effectiveness, divergence, and control system reversal; dynamic aeroelastic phenomena include flutter, buffet, dynamic response, and aeroelastic effects on dynamic stability [1]. The present work is concerned with flutter which is defined as dynamic aeroelastic instability.

Early considerations of aeroelastic effects in the design process were in response to observed issues and involved limited understanding of the relevant physics [1]. By 1935, Theodorsen [2] had developed a method to calculate flutter of three degree of freedom models including bending, torsion, and aileron deflection where the unsteady aerodynamics are calculated using potential flow theory and Bessel functions. By 1955, methods were extended to include prediction of more complex structural dynamics through the use of the Rayleigh Ritz method, and more general aerodynamic characterization through the use of strip theory [1]. By 1979, the combination of Doublet-Lattice aerodynamics [3] with Finite Element structural models was made available resulting in a system for analysis of more general aircraft configurations including models exhibiting plate modes [[4]]. In recent decades, advances in aerodynamic analysis have included extension to higher fidelity aerodynamic characterizing viscous and compressibility effects [5], [6], as well as improved structural dynamic methods characterizing structural nonlinearities [7], [8], [9], [10].

In order to achieve high operating efficiency, HALE aircraft configurations tend to be designed to be flexible, high aspect ratio, flying wings. Such configurations tend to be susceptible to aeroelastic instability in which the flexible modes of the vehicle couple with the rigid body flight dynamic modes. This has been documented for the B-2 bomber which is a flying wing configurations addressing conventional mission. The B-2 exhibited residual pitch oscillation due to coupling of short period and first bending modes in flight that was not well predicted [11]. A

<sup>\*</sup> Vice President of Engineering, Member, AIAA.

<sup>†</sup> Staff Engineer, Member, AIAA.

<sup>‡</sup> President, Member, AIAA.

<sup>§</sup> Engineer .

particularly noteworthy incident was the loss of the Helios aircraft due to oscillatory coupling of phugoid and elastic modes. This mishap led to a call for more advanced simulation methods capable of predicting such complex instability mechanisms [12]. Significant and valuable work has been done developing methods for simulating nonlinear aeroelastic behavior with coupled rigid body and elastic motion for HALE configurations. This includes demonstration of the significance of nonlinear effects through computational results [13], [14], examination of design implications [15], and comparisons to experimental studies [16], [17].

Throughout the literature on high aspect ratio flying wing configurations, nonlinear geometric effects as well as coupling of flexible and rigid body modes have consistently been found to be significant. In the current work, an incremental approach is taken where analysis initially focuses on linear aeroelastic analysis with free body boundary conditions. Subsequent analysis includes a linearized representation of the altitude speed coupling necessary for capturing the phugoid mode. An optimization study is conducted to identify candidate designs to address mass and drag objectives while satisfying an aeroelastic stability requirement. Simulation of dynamic aeroelastic behavior with geometric nonlinearities is left for future work.

## II. Technical Approach

### A. Analysis

#### 1. Structural Finite Element Model

The beam representation finite element model was used. The beams extended spanwise along the flexural axis and represented the structure. The beams were prescribed stiffness and mass properties interpolated from the defined stations. Bar elements extended chordwise from the leading edge to the trailing edge. These bars were connected by the rigid body elements to the spar beams. The bars served to transfer the aerodynamic loads to the spar beams and to aid in result visualization. The winglets were modeled in a similar fashion. Concentrated mass elements were used to represent the payload and motors. The elevon structures were modeled with point mass elements to match the inertia estimates and attached to the wing spring elements of the estimated stiffness. Figure 1 shows the structural model. The mass, CG, and moment of inertia of the model were compared to reference values for the configuration.

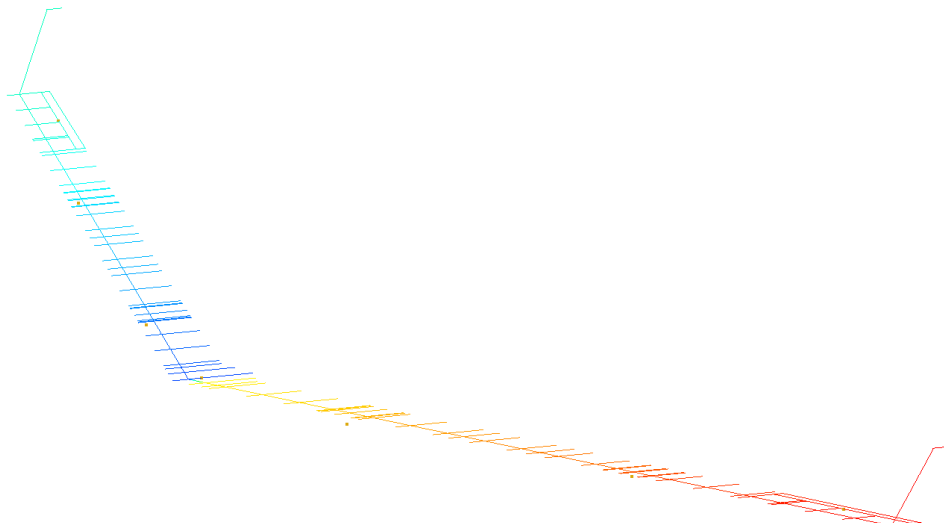


**Figure 1: Structural Model**

#### 2. Aerodynamic Models

Doublet-Lattice and strip theory aerodynamic models were constructed representing the aerodynamic behavior of the wing and winglets. The initial panel incidence angles were determined by the camber line of the airfoil and the twist angle at each spanwise station. Elevons were modeled with aerodynamic panels as called out in the design. The Doublet-Lattice aerodynamic model can be seen overlaid on the structural model in Figure 2.

The vehicle aerodynamic coefficients from Doublet-Lattice were compared to those from Navier-Stokes CFD simulations. While the lift and pitching moment curve slopes correlated well with CFD data, the intercepts were somewhat different. In order to correct the aerodynamic model, an additional twist and camber correction was

applied to each panel. The camber angle correction was based on a quadratic chordwise distribution. The twist angle correction was constant for every panel.

$$\text{camber angle correction} = a \frac{x}{c} \left( \frac{x}{c} + \frac{1}{2} \right)$$

$$\text{twist angle correction} = t$$

An optimization was performed to determine the values of  $a$  and  $t$  to match the rigid aerodynamic coefficients to the CFD lift and pitching moment intercepts. Loads and trim analyses were performed using the twist and camber corrections. The twist and camber corrections do not affect flutter analysis

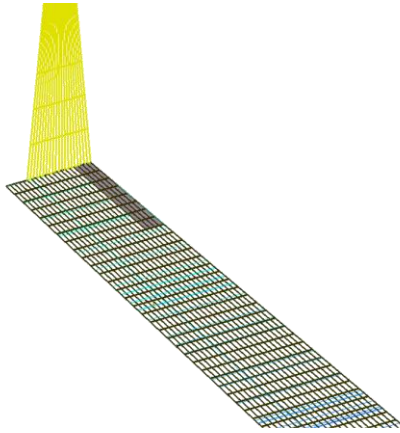


**Figure 2: Aerodynamic Model**

### 3. Aeroelastic Eigenvalue Determination

Three methods were used for aeroelastic eigenvalue calculation. These methods each have advantages in terms of what physical phenomena are captured and are discussed here.

The first method was application of the PK flutter method in MSC Nastran as described in Reference [18]. This method iteratively converges the frequency of the aerodynamic and structural motion and determines the damping required to enforce harmonic oscillation. This method was applied using both Doublet-Lattice and strip theory aerodynamic models. While rigid body motion was unconstrained, this approach does not include the interaction between altitude and speed required to capture the phugoid mode. Additionally, simulations were performed as linear in the frequency domain and as such did not include large deformation nonlinearities.

The second method applied was based on extraction of DLM based aeroelastic models using M4 Reduced Order Model generation software [19]. In this approach, the modal unsteady aerodynamic transfer functions were fit using Roger's Rational Function Approximation (RFA) process [20]. These models were then augmented to equations for six degree of freedom simulation that include gravity, propulsion, and Coriolis terms. The Jacobian of these models is computed to generate a linear state space representation of the coupled dynamics. The eigenvalues of the resulting state propagation matrix are computed. While this modeling approach is capable of representing phugoid dynamics it does not include large deformation nonlinearities.

The third method applied is inclusion of a strip theory aerodynamic element into the Abaqus nonlinear commercial finite element solver. This element was developed to compute current forces based on the history of motion as described in Reference [2]. Using this approach, simulations are performed in the time domain and system identification is performed on the resulting motion to identify modal behavior. Initial simulations have been focused on linear models, however this approach is extensible to include nonlinear effects due to large rotations.

### 4. Trim Drag Model

To determine the drag due to trim for use in the objective function, a drag model was built. The primary concerns for drag were the trim deflection of the elevons and change in cruise induced drag. The representative cruise condition of steady level flight was chosen as the trim condition.

An approximation of the viscous trim drag was developed based on a sectional drag calculation for the portions of the wings where the elevons are located.

$$\Delta D_v = qS_e\Delta C_D = qb_e c_e \Delta C_D$$

$$\Delta C_D = f(\delta_{trim})$$

Where  $q$  is the free stream dynamic pressure,  $S_e$  is the planform area of the elevon portion of the wing, and  $\delta_{trim}$  is the elevon deflection required for trim.

The function  $\Delta C_D = f(\delta_{trim})$  was fit to data from Xfoil simulations. The 80% semi-span station and 100% semi-span station airfoils were studied over a range of deflections and angles of attack.

Xfoil analysis of viscous flow at was performed for angles of attack between -16 and 20 degrees angle of attack and elevon deflection between 10 degrees down and 20 degrees up.  $C_D$  vs. elevon deflection results for angle of attack of 4 degrees is shown in Figure 3. A comparison with experimental  $C_D$  vs.  $\delta$  for a similar airfoil, the MS 0313, are also shown [21]. The quadratic fit was used to estimate the  $\Delta C_D$ .

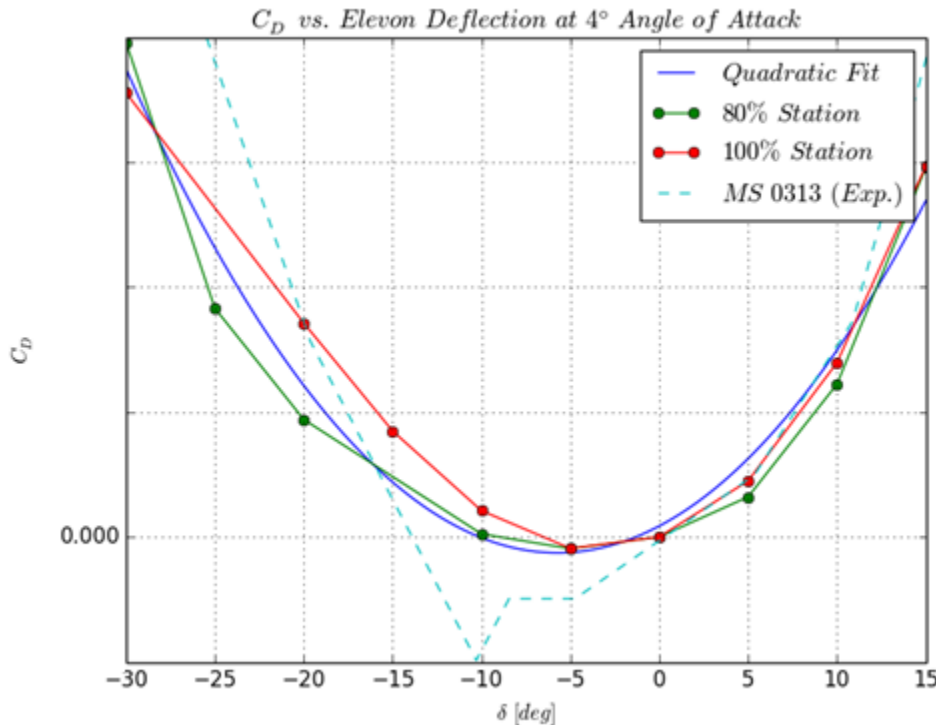


**Figure 3: CD vs. Elevon deflection at 4 degrees angle of attack for 80% and 100% span station airfoils. Experimental data from [21]**

Induced drag was modeled using a lifting line theory code. Aerodynamic loading was extracted from the aerodynamic box forces at the trim condition. They were assembled into chordwise strips representing the wing and winglets as seen in Figure 4. The induced drag was computed for the baseline and for each design in the optimization. The difference between the candidate design induced drag and the baseline induced drag was added to the  $\Delta D$  for the objective function.

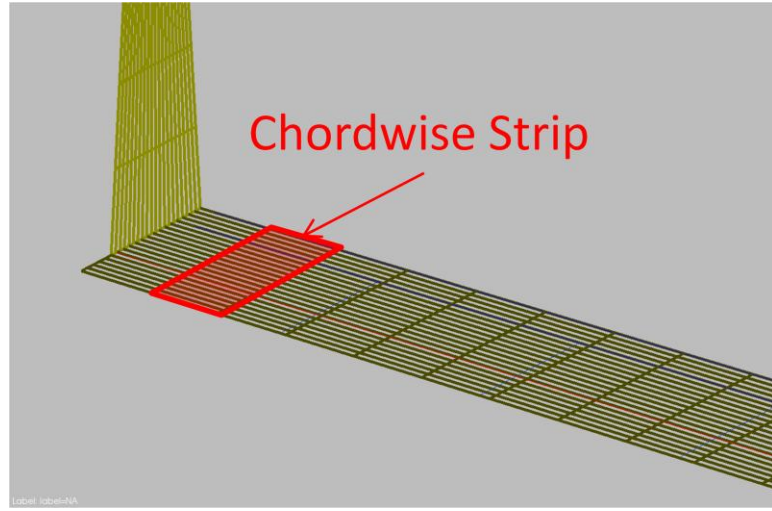


**Figure 4: Chordwise strip aerodynamic model for lifting line theory**

## B. Optimization

### 1. Approach

An optimization was performed to analyze the effect of possible design changes to eliminate open-loop flutter from the flight envelope. The design variables were the flatwise bending stiffness and the chordwise center of gravity locations of the motors. A representative objective function of additional mass and additional drag due to trim was minimized for the optimization. Models for drag due to trim elevon deflection and mass of additional stiffeners were developed. Constraints were added to ensure no open loop flutter and restrict the choice of design variables. Optimization was performed using both a gradient based solver, and a Genetic Algorithm implemented in Python.

In order to provide a set of choices for possible design modifications, optimizations were performed with several variations of objective function. Various drag weighting constants were used in the objective function to achieve different optimized designs. A Pareto frontier was constructed to represent the design space encompassed by this approach.

### 2. Objective Function

The objective function represented a system scale penalty due to the studied design modification. This function was minimized to obtain an optimal design. The objective function was defined by cruise power required for steady level flight. The function is defined below:

$$P = V_c D$$

Where  $P$  is the power,  $V_c$  is the cruise speed,  $D$  is the drag.

Cruise speed was estimated with the following relation.

$$V_c = V_{c0} \left( \frac{m}{m_0} \right)^{0.5}$$

Where  $V_{c0}$  is the baseline cruise speed,  $m$  is the mass and  $m_0$  is the baseline mass.

The function was chosen as it represents the major physical mission-scale costs of changing the design variables available. The drag includes induced drag, viscous drag due to trim elevon deflection, and other parasitic drag. The induced drag changes with both the mass of the design and with the trim elevon deflection as the spanwise lift distribution is changed. The other parasitic drag was neglected for the optimization.

### III. Results

#### A. Wind-Off Modal Analysis

A modal solution is performed on the optimum design. The resulting mode shapes are shown in Figure 5. The first symmetric bending mode is of significant importance for the aeroelastic behavior. Note that the wind off mode contains significant vehicle pitch motion due to the sweep of the wing.

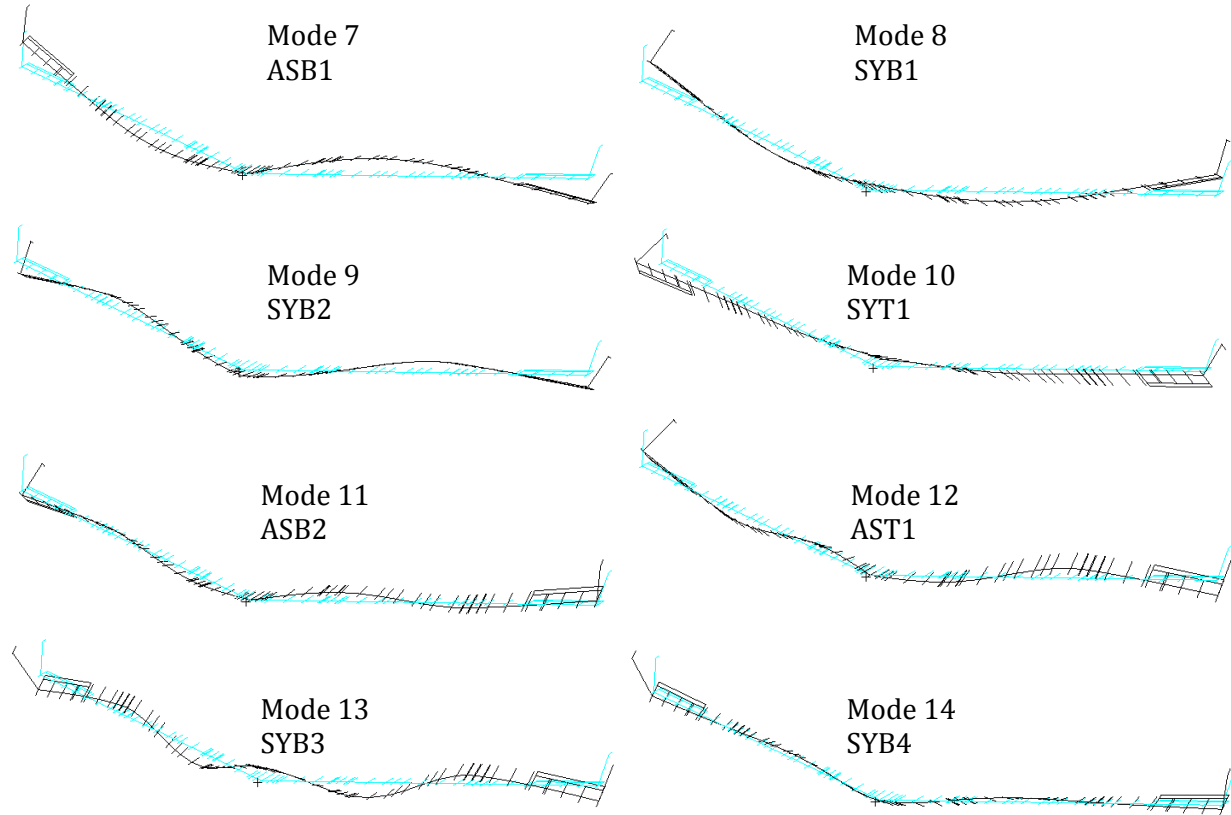
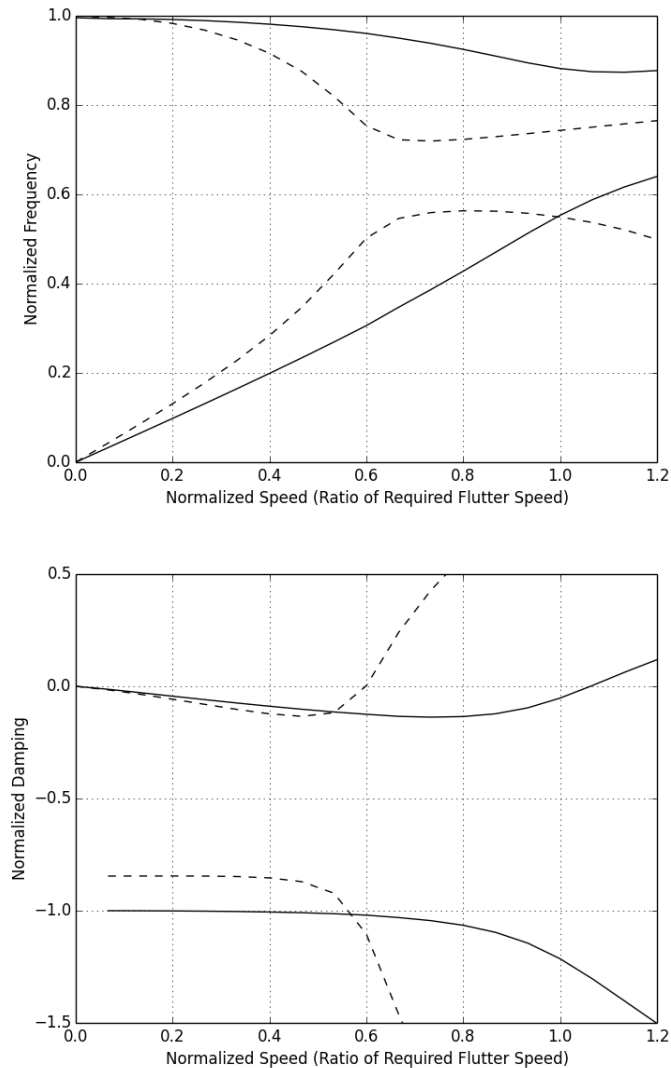


Figure 5: Wind-off mode shapes.

#### B. Flutter Analysis

##### 1. Linear Doublet-Lattice Results

Aeroelastic stability analysis of the baseline and optimized configuration has been performed over a range of altitudes. Analysis was performed using the PK-Flutter method. At each altitude, a number of flight conditions of varying speed were studied. A plot of the modal frequency and the damping required to achieve harmonic motion as a function of airspeed for the critical altitude is given in Figure 6. The speed at which the damping crosses from negative to positive is the flutter speed. The optimized configuration satisfies the constraint by having a normalized flutter speed above unity. Note that while the wind off frequency of the first elastic mode does not change significantly there is a noticeable change in the mode shape (Figure 7). The change in the flutter speed is thus attributed to change in the mode shape. The aeroelastic mode shape at a speed slightly beyond the flutter boundary is shown in Figure 8.



**Figure 6: Aeroelastic modal behavior for baseline (dashed) and optimized (solid) configurations.**

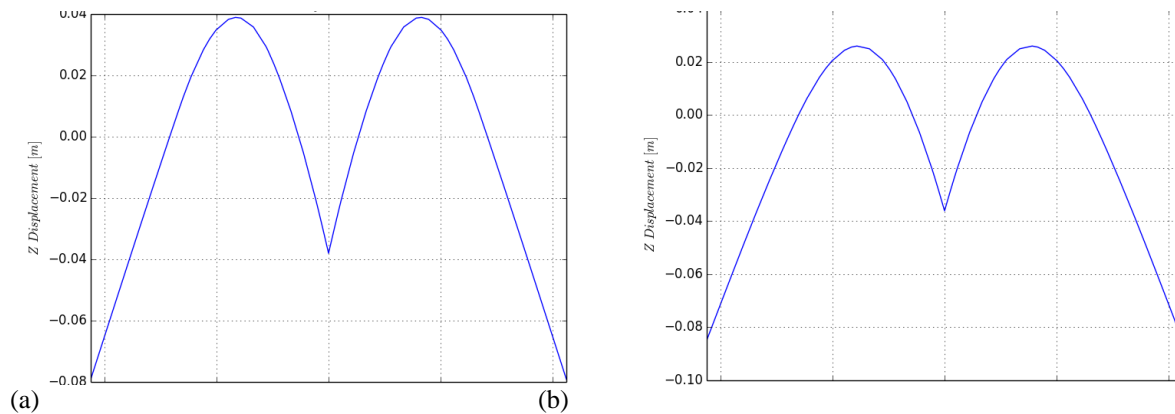


**Figure 7: Comparison of Wind-Off Mode Shapes for (a) Optimal and (b) Alternate Design.**

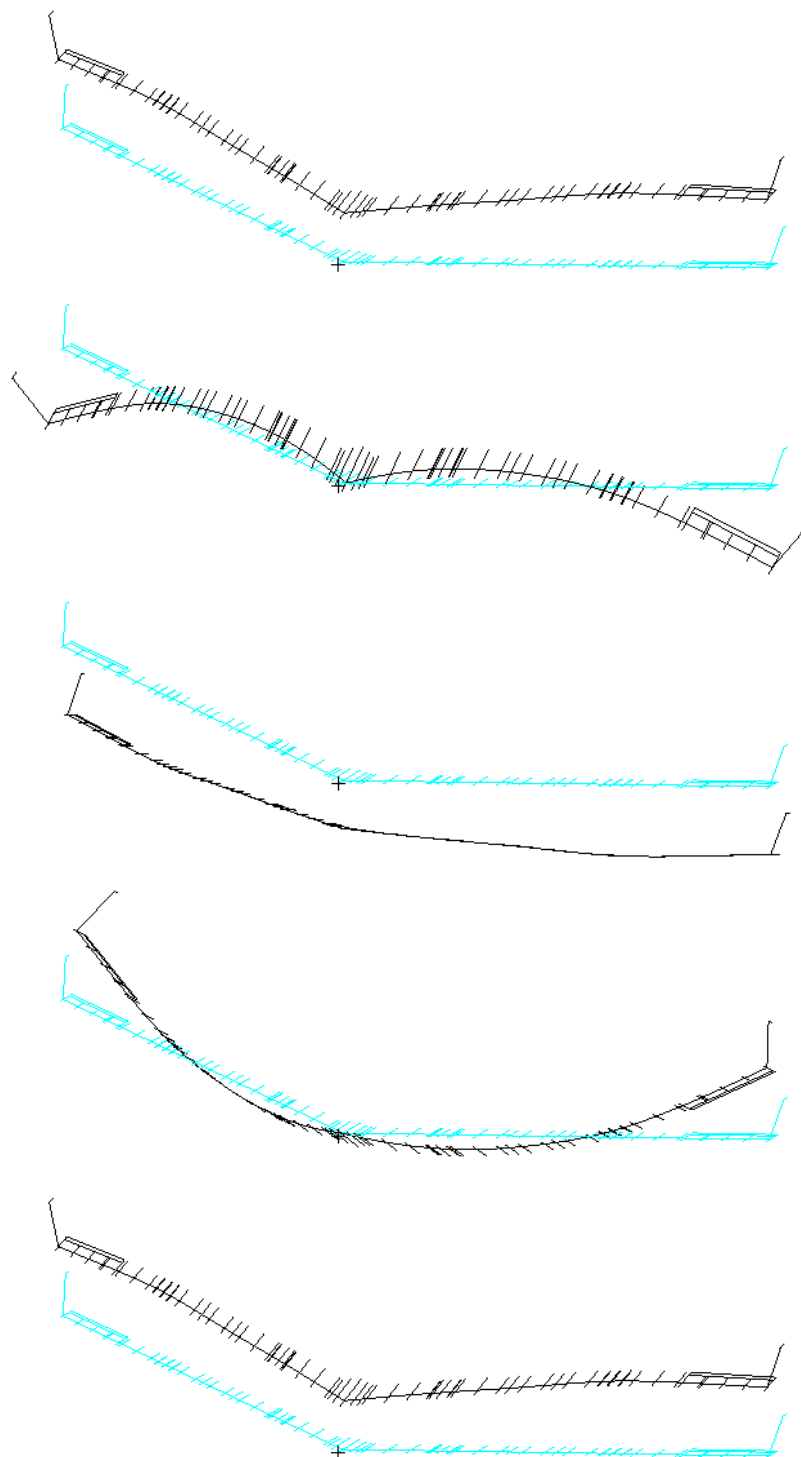


**Figure 8: Flutter mode shape.**

## 2. Comparison of Results for Multiple Analysis Methods

In order to gain confidence in the analysis results, simulations were performed with multiple methods. This includes the PK frequency domain method in Nastran using the DLM and strip theory models and the time domain method in Abaqus using the user created aerodynamic strip element. The results are shown in Figure 9 and indicate a difference between Doublet-Lattice and strip aerodynamic methods. There is agreement among the frequency and time domain methods. Note that the time domain simulations to date include linear assumptions. The difference noted comparing Doublet-Lattice to strip results indicates that uncorrected strip theory aerodynamics appear inadequate for accurately representing the system behavior with nonlinear models.

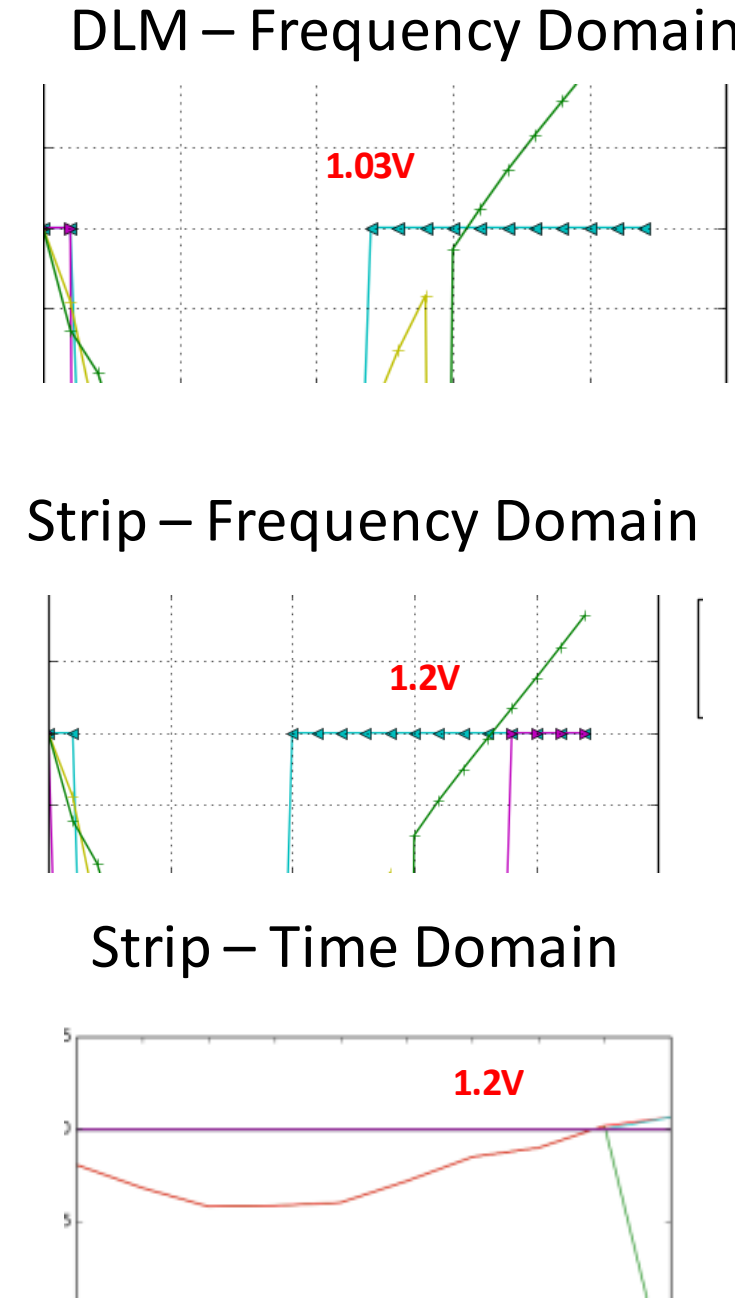
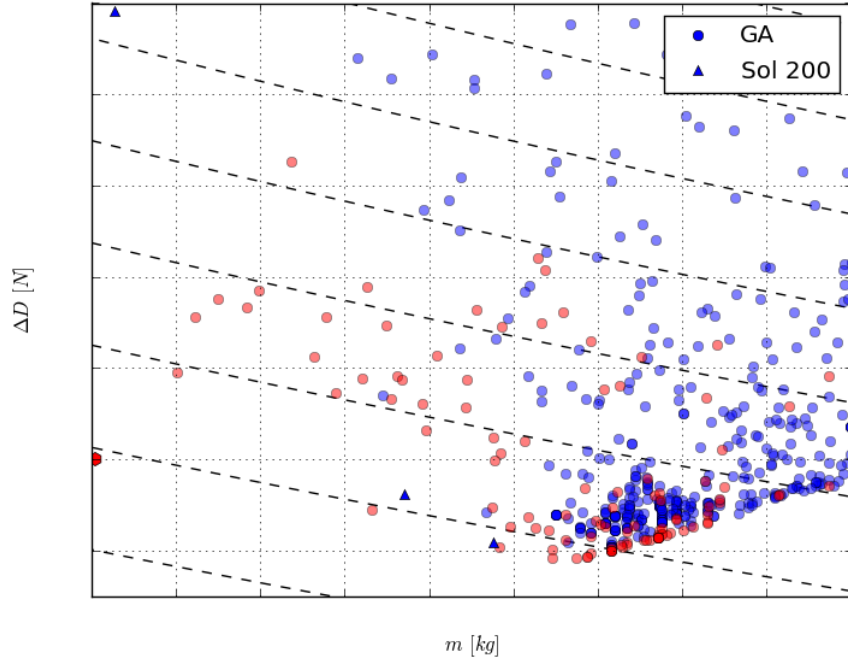


Figure 9: Damping vs speed comparison for various methods.

### C. Optimization Results

The result of the optimization process was thousands of possible designs, some of which had flutter in the flight envelope. Each design is plotted against its mass and drag increment in Figure 10. Designs with no flutter at the design condition are represented by blue points. Red points represent designs that were predicted to have flutter at the design condition. Designs from the gradient based optimization processes are triangles while designs from the genetic algorithm are dots. The baseline configuration is the red dot in the lower left. The Pareto Frontier is made up of the lower-left-most blue designs.



**Figure 10: Flutter optimization Pareto frontier with infeasible designs**

For the optimal design with no change in mass, the blue triangle in top left corner, a large drag penalty was incurred. This was due to the large elevon deflections necessary to counter the moment induced by moving the motors forward. Following the frontier down and to the right, the designs added stiffness through the carbon fiber plies and moved the overall vehicle CG less, requiring a smaller trim elevon deflection and thus inducing less drag. The frontier does not reach 0  $\Delta D$  because the higher mass designs required a larger  $C_L$  to trim and thus generated more induced drag.

As all of the designs along a Pareto Frontier are optimal with respect the parameters of the frontier, mass and  $\Delta D$  in this case, another metric was necessary to narrow the frontier to one design. An estimate of the percent power increase relative to the baseline design was made based on the drag and mass increments.

In Figure 11, only designs without flutter at the design condition are shown. Contours of the percent power increase are also shown. The baseline configuration is also listed for comparison. The selected design is circled in green.

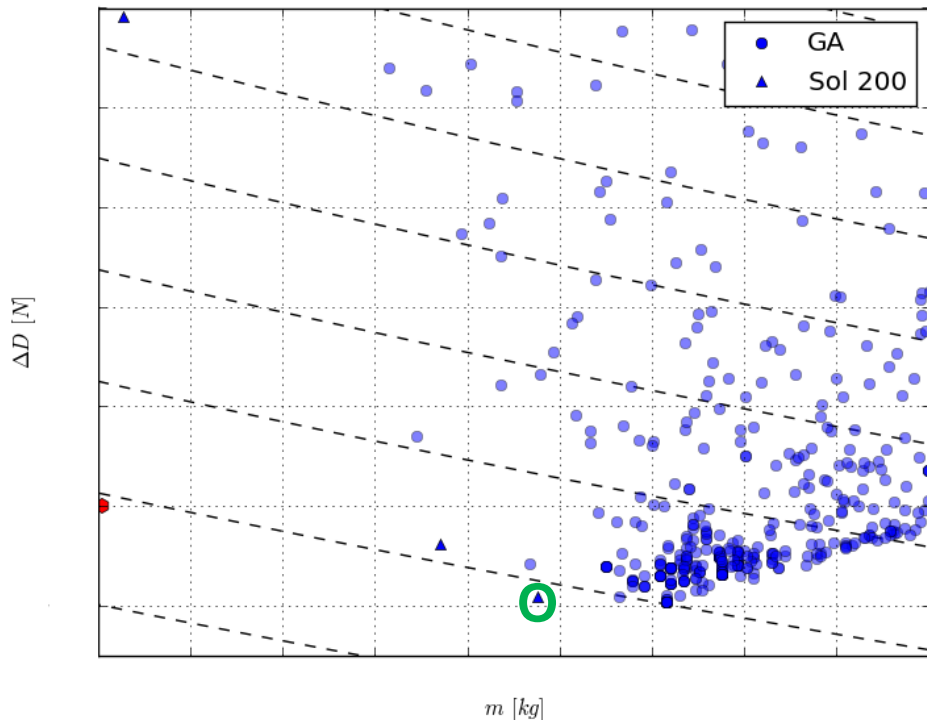


**Figure 11: Flutter optimization Pareto frontier with %Power contours**

#### IV. Conclusion

A flutter analysis has been performed on a generic HALE aircraft configuration. Design variables included chordwise location of motor masses and added stiffness. A Pareto frontier of mass and drag was found for designs that satisfy a flutter constraint. The optimal design was found to have a small impact on the wind-off frequency of the first bending mode. Comparison of flutter predictions using multiple methods indicates that finite span effects have a significant impact on the flutter speed.

#### References

1. Bisplinghoff, R. A., Ashley, H., and Halfman, R. L. *Aeroelasticity*. Toronto : Dover, 1955.
2. Theodorsen, T. *General Theory of Aerodynamic Instability and the Mechanism of Flutter*. 1935. NACA Report 496.
3. Giesing J. P., Kalman T.P., and Rodden W.P. *Subsonic unsteady aerodynamics for general configuration*. 1971. AFFDL-TR-71-5.
4. Rodden, W. P., Harder, R. L., and Bellinger, E. D. *Aeroelastic Addition to NASTRAN*. 1979. NASA CR-3094.
5. Bendiksen, O. O. *Role of Shock Dynamics in Transonic Flutter*. Dallas, TX : AIAA Dynamics Specialists Conference, Apr. 1992. pp. 401-414. AIAA-1992-2121.
6. Silva, W. A. *Modeling Transonic Aerodynamic Response using Nonlinear Systems Theory for use with Modern Control Theory*. s.l. : NASA LaRC Workshop on Guidance, Navigation, Controls, and Dynamics for Atmospheric Flight, 1993.
7. Dowell, E. H. and Tang, D. *Nonlinear Aeroelasticity and Unsteady Aerodynamics*. 9, s.l. : AIAA Journal, 2002, Vol. 40.
8. Seber, G., and Bendiksen, O. O. *Nonlinear Flutter Calculations Using Finite Elements in a Direct Eulerian-Lagrangian Formulation*. 6, s.l. : AIAA Journal, 2008, Vol. 46.
9. Livne, L. and Demasi, E. *Aeroelastic Coupling of Geometrically Nonlinear Structures and Linear Unsteady Aerodynamics: Two Formulations*. Schaumburg, IL : 49th AIAA Structures, Structural Dynamics, and Materials Conference, Apr. 7-10, 2008. AIAA-2008-1758.

10. Livne, L. and Demasi, E. *Dynamic Aeroelasticity Coupling Full Order Geometrically Nonlinear Structures and Full Order Linear Unsteady Aerodynamics - The Joined Wing Case*. Schaumburg, IL : 49th AIAA Structures, Structural Dynamics, and Materials Conference, Apr. 7-10, 2008. AIAA-2008-1818.
11. Jacobson S., Britt R., Freim D., Kelly P. *Residual Pitch Oscillation (RPO) Flight Test and Analysis on the B-2 Bomber*. s.l. : AIAA Structures, Structural Dynamics, and Materials Conference, 1998. AIAA-98-1805.
12. Noll, T.E., Brown, J.M., Perez-Davis, M.E., Ishmael, S.D., Geary, G.C., Gaier, M. *Investigation of the Helios Prototype Aircraft Mishap*. s.l. : NASA, January, 2004.
13. Patil, M., Hodges, D., Cesnik C. *Nonlinear Aeroelasticity and Flight Dynamics of High-Altitude Long-Endurance Aircraft*. 1, s.l. : AIAA Journal of Aircraft, Vol. 38.
14. Patil, M.J., Hodges, D.H. *On the importance of aerodynamic and structural geometrical nonlinearities in aeroelastic behavior of high-aspect-ratio*. s.l. : Journal of Fluids and Structures, 2004, Vol. 19.
15. Cesnik, C, Palacios, R, Reichenbach, E. *Reexamined Structural Design Procedures for Very Flexible Aircraft*. s.l. : Journal of Aircraft, 2014, Vol. 51. 10.2514/1.C032464.
16. Britt, R, Ortega, D., McTigue J., Scott, M. *Wind Tunnel Test of a Very Flexible Aircraft Wing*. Honolulu : AIAA Structures, Structural Dynamics and Materials Conference, 2012. AIAA 2012-1464.
17. Cesnik C., Senatore P., Su W., Atkins E., Shearer C. *X-HALE: A Very Flexible Unmanned Aerial Vehicle for Nonlinear Aeroelastic Tests*. 12, s.l. : AIAA Journal, 2012, Vol. 50.
18. MSC Software Corporation. *MSC Nastran Aeroelastic Analysis User's Guide*. Santa Ana, CA : s.n., 2004.
19. Roughen, K.M., Bendiksen, O.O, and Baker, M.L. *Development of Generalized Aeroviscoelastic Reduced Order Models*. Palm Springs, CA : 50th AIAA Structures, Structural Dynamics, and Materials Conference, 2009.
20. Roger, K. L. *Airplane Math Modeling Methods for Active Control Design*. s.l. : AGARD-CP-228 Structural Aspects of Active Controls, Aug. 1977.
21. Wentz Jr., W. H. *Wind Tunnel Force and Pressure Tests of a 13% Thick Medium Speed Airfoil With 20% Aileron, 25% Slotted Flap and 10% Slot-Lip Spoiler*. Wichita State University. Wichita, Kansas : s.n., 1981. NASA Contractor Report 3439.